Evolution of a curved vortex filament into a vortex ring

Parviz Moin, Anthony Leonard, and John Kim
NASA Ames Research Center, Moffett Field, California 94035

(Received 26 September 1985; accepted 18 December 1985)

The deformation of a hairpin-shaped vortex filament under self-induction and in the presence of shear is studied numerically using the Biot–Savart law. It is shown that the tip region of an elongated hairpin vortex evolves into a vortex ring and that the presence of mean shear impedes the process. In addition, evolution of a finite-thickness vortex sheet under self-induction is investigated using the Navier–Stokes equations. The layer evolves into a hairpin vortex, which in turn produces a vortex ring of high Reynolds stress content. These results indicate a mechanism for the generation of ring vortices in turbulent shear flows, and a link between the experimental and numerical observation of hairpin vortices and the observation of Falco [Phys. Fluids **20**, S124 (1977)] of ring vortices in the outer regions of turbulent boundary layers.

I. INTRODUCTION

Hairpin-shaped vortices (also referred to as horseshoe vortices) are commonly proposed as the characteristic organized structures in turbulent boundary layers.[1–5] Recently, using vorticity fields generated by large-eddy simulation, Moin and Kim[6] demonstrated that turbulent channel flow contains an appreciable number of hairpin vortices often inclined at 45° to the flow direction. It was also shown that hairpin vortices are associated with the bursting process, thus indicating their importance in the turbulence energy production mechanism.[7] The same structures are found in homogeneous turbulent shear flow[8] and this implies that hairpin vortices are the characteristic structures not only in turbulent boundary layers, but in *all* turbulent shear flows.

Falco[9] identified a relatively small-scale coherent motion, which he labeled "typical eddy," in the outer region of a smoke-filled, turbulent boundary layer. Using simultaneous hot-wire anemometry and flow visualization, Falco[10] showed that these eddies produce most of the Reynolds stress in the outer region. Falco's reported visualizations are generally in a plane parallel to the flow and perpendicular to the wall (x-y planes), but he does present sketches of the typical eddy in planes perpendicular to the wall and the flow direction (y-z planes). Figure 1 shows Falco's sketch of two views of the typical eddy. He points out that "sometimes only the solid outline [in Fig. 1(a)] is observed, but at other times the outline of the typical eddy consists of both the solid and dashed lines." Because the cross-section outline (in an x-y plane) of a vortex ring inclined to the flow direction resembles the *complete* outline of the sketch in Fig. 1(a), Falco identifies the typical eddy as a vortex ring. It should be pointed out, however, that the cross-section outline of a hairpin vortex would resemble the solid line in Fig. 1(a).

A relevant computational work is that of Hama,[11] who studied the deformation of an initially parabolic vortex filament by using the localized induction concept. His calculations show that the lifted portion of the filament progressively assumes circular shapes resembling part of a ring vortex. Using the more accurate Biot–Savart induction law, Dhanak and De Bernardinis[12] demonstrated that an initially elliptic vortex ring of relatively high eccentricity breaks up into two smaller loops, but that an elliptic vortex of low eccentricity may simply oscillate without pinch-off.

The common feature of the hairpin vortices observed in the simulations of Moin and Kim[6] was the bottleneck, or Ω shape, of their tip region. This observation and the results of Hama led the authors to speculate that the hairpin vortices observed in the turbulent shear flows may pinch off into ring vortices, thus providing a mechanism for the generation of ring vortices in turbulent shear flows and a link between the ring vortices observed by Falco and the hairpin vortices observed (or conjectured) by others.

The objective of this study is to examine the motion of a curved vortex filament or a hairpin vortex under its self-induction and in the presence of mean shear. We were particularly interested in determining whether the hairpins pinch-off into ring vortices and, if so, what factors influence this process. This article extends Hama's work as follows: Hama used the local-induction approximation, which neglects the contribution to the velocity from other portions of the vortex. In the present work the velocity is calculated using the full Biot–Savart line integral and also by means of three-dimensional Navier–Stokes equations. In the Navier–Stokes computations, we examine the evolution of a perturbed layer of vorticity in a channel. Such perturbations to the mean flow naturally occur in turbulent shear flows, and

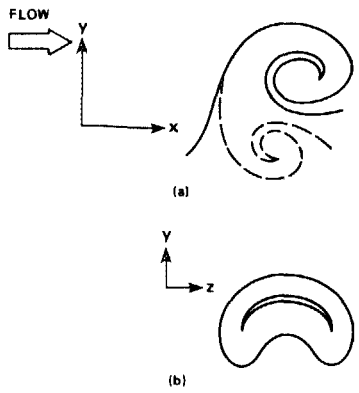

FIG. 1. Sketches of the organized structures in the outer layer by Falco.[10] (a) Side view; (b) front view.

 0031-9171/86/040955-09$01.90

it has been conjectured that they evolve into hairpin vortices[6] that in turn may generate vortex rings. In contrast to the Biot–Savart computations, in the Navier–Stokes calculations the viscous effects are accounted for, which are significant when vortices of opposite signs merge in the pinching process. Hama's work did show the evolution of a curved vortex filament into the Ω shape, but his calculations were not carried far enough to indicate the possible occurrence of pinch-off. The filament may oscillate about a configuration as has been shown for an elliptic vortex ring by Dhanak and De Bernardinis.[12] In any case, it is doubtful that the local-induction approximation could lead to meaningful results when the vortex cores approach each other in the splitting process. One may consider three stages in the pinching process: the early stage where the local induction effects are dominant, the stage during which the influence of the neighboring vortices is important, and the final period where viscous stresses become significant. The Biot–Savart calculations encompass the first two, and the Navier–Stokes calculations encompass all three. We will also present the effects of a background shear flow and the presence of a wall on the evolution of the vortex filament. Finally, we will use our results to propose a model for the structure of the vorticity field in turbulent shear flows.

II. NUMERICAL METHODS

In the Lagrangian (Biot–Savart) calculations, we assume that the vorticity field is in the form of a tube of concentrated vorticity following the space curve $\mathbf{r}(\xi,t)$ plus weak background vorticity producing a mean shear. The motion of the space curve is determined by self-induction plus an external component,

$$\frac{\partial \mathbf{r}}{\partial t} = -\frac{\Gamma}{4\pi} \times \int \frac{[\mathbf{r}(\xi,t) - \mathbf{r}(\xi',t)] \times (\partial \mathbf{r}/\partial \xi') g(|\mathbf{r} - \mathbf{r}'|)}{|\mathbf{r} - \mathbf{r}'|^3} \times d\xi' + U(\mathbf{r},t), \tag{1}$$

where U is the background velocity, Γ is the circulation of the vortex tube, and the function g models the effect of distributed vorticity within a core of effective radius σ (see Ref. 13). The equation of motion is valid in the thin-filament approximation: the structure of the core remains nearly constant in time and the disturbance wavelengths are larger than the core radius. In addition, we neglect the generation of new disturbance vorticity produced by the velocity field of the hairpin vortex acting upon the background vorticity (see Sec. III C).

For numerical purposes, the space curves were tracked by following a sequence of node points on the curve. The function g was taken to be

$$g(y) = y^3/(y^2 + \alpha\sigma^2)^{3/2},$$

with $\alpha = 0.413$ (Ref. 14) corresponding to the Gaussian core vorticity

$$\omega(r) = (\Gamma/\pi\sigma^2)e^{-r^2/\sigma^2}.$$

Integration along the curve was performed by the midpoint rule and second-order central differencing was used to estimate $\partial r/\partial \xi'$. The time-integration method was third-order Runge–Kutta.

The spacing between the node points, Δ, was sufficiently small so that length scales of interest would be represented accurately. In particular, if the initial minimum radius of curvature of the hairpin vortex is ρ_0, then

$$\Delta < \rho_0. \tag{2a}$$

On the other hand, the cutoff scheme used in the thin-filament approximation generally produces (even in the absence of numerical errors) spurious results for length scales smaller than σ.[14] These spurious small scale motions can lead to inaccuracies in the dynamics of the large scale motions as illustrated by the analysis of the motion of a rectilinear vortex having a constant vorticity core.[14] They may also lead to numerical instabilities because of their small time scales, but these can be controlled by time step reduction. To prevent the appearance of the spurious small scales, the constraint

$$\Delta > 2\sigma \tag{2b}$$

was also enforced.[14]

A pseudospectral method was used for the Navier–Stokes computations.[15] The flow is assumed to be between two parallel plates and is maintained by a mean pressure gradient. No-slip boundary conditions are enforced on the plates, and the flow is periodic in the streamwise and spanwise directions. In the direction normal to the walls, y, the flow field is represented by a series of 129 Chebyshev polynomials. Fourier series with 128 modes are used in each of the streamwise and spanwise directions. Thus, a total of about 2×10^6 collocation points were used. Time is advanced by a second-order semi-implicit scheme.

The Biot–Savart computations are initialized with a thin filament of concentrated vorticity, whereas the initial condition for the Navier–Stokes computations is a perturbed layer of vorticity. Note that no attempt is made to reproduce that results of the Biot–Savart calculations with the Navier–Stokes computations. Such a study would require an adaptive time-dependent clustering of grid points about the vortex filament.

III. RESULTS AND DISCUSSION

The results presented in Secs. III A–III C are obtained using the Biot–Savart law and those in Sec. III D are obtained using the Navier–Stokes computations. The flow is in the x direction, y is the direction normal to the wall(s), and z is the spanwise direction.

A. Evolution of an isolated parabolic vortex

The initial configuration of the vortex filament is the parabola $x = -az^2$; $y = 0$. The constant a has the dimension of inverse length. This filament is isolated in space; that is, the effects of shear or image vortices accounting for the wall impermeability are not included. Note that in our calculations [when $U = 0$ in Eq. (1)] the actual value of the circulation Γ is not significant, since it can be absorbed into a rescaling of the time variable; the only nondimensional length parameter is σa. We are assuming that our vortex

filament is formed from the roll-up of a sheet of vorticity in a turbulent boundary layer (see Sec. III D). The radius of the vortex core is specified to be $\sigma = 0.125$. In Fig. 2, the evolution of the filament with $a = 1$ is shown. At each instant in time, the plan, side, and end views are presented. The range of the variable z was from $z = -20$ to $z = 20$, with x ranging from 0 to -400. The large range of the independent variables is used to minimize the effects of artificially terminating the vortex filament on the deformation of the tip region. It will be shown that such deformations are confined to

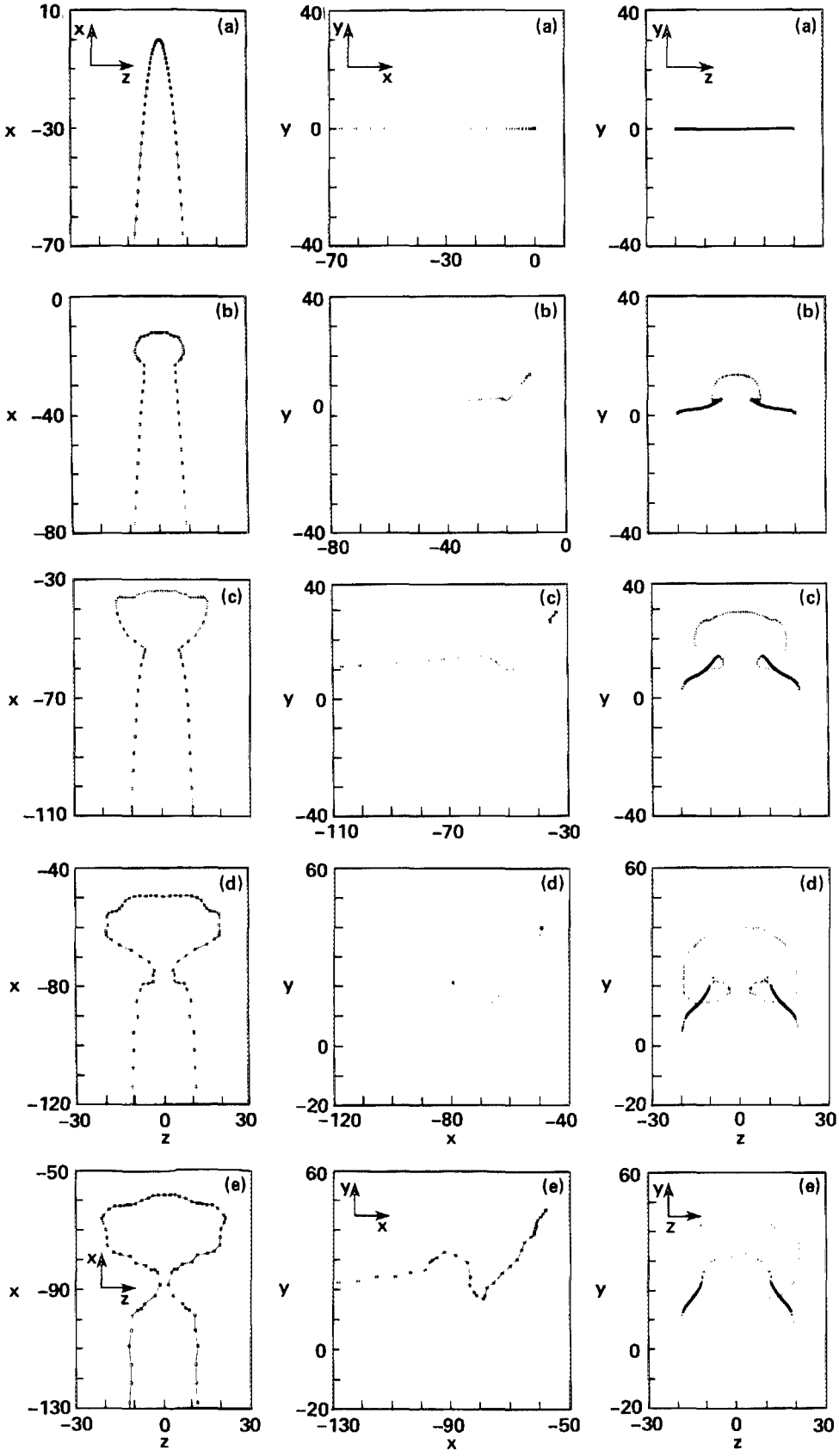

FIG. 2. Evolution of the parabolic vortex filament $x = -z^2$, $\sigma = 0.125$. Plan views are in the left column, the middle column shows the side views and the end views are shown in the right column: $ta^2\Gamma$ = (a)0; (b) 7.1×10^3; (c) 2.8×10^4; (d) 5.0×10^4; (e) 6.5×10^4. The symbols indicate the location of the node points.

$\Delta x \simeq 50$ in the tip region and hence unaffected by the end conditions. The filament is represented by $N = 129$ elements uniformly spaced in the z direction. The relatively small core size and the value of N are chosen in accordance with the accuracy requirements [Eqs. (2a) and (2b)].

The small radius of curvature in the tip region ($\rho = 1/2a = 0.5$) results in the rapid rise of the tip above the x-z plane, giving a three-dimensional configuration to the vortex. Gradually, other portions of the vortex in the vicinity of the tip also rise. It appears that the raised portion has approximately uniform velocity in the x-y plane. This is because the subsequent cross sections of the filament in this plane are approximately parallel to each other. As the tip region lifts from the plane of the initial filament, secondary curvature is introduced between the legs and the tip. This curvature in x-y plane induces a z-velocity component which forces the legs away from each other and leads to the bulged-out shape, or Ω shape, evident in the plan and end views of Fig. 2. The curvature in the x-y plane and the subsequent velocity in the z direction create a curved section in the x-z plane leading to negative velocity in the y direction and to the corresponding downward movement of the filament in the transition regions between the legs and the tip. The resulting curvature in the x-y plane induces opposite velocites on each leg in the z direction, forcing them toward each other and causing pinch-off. The plan and end views show that the tip

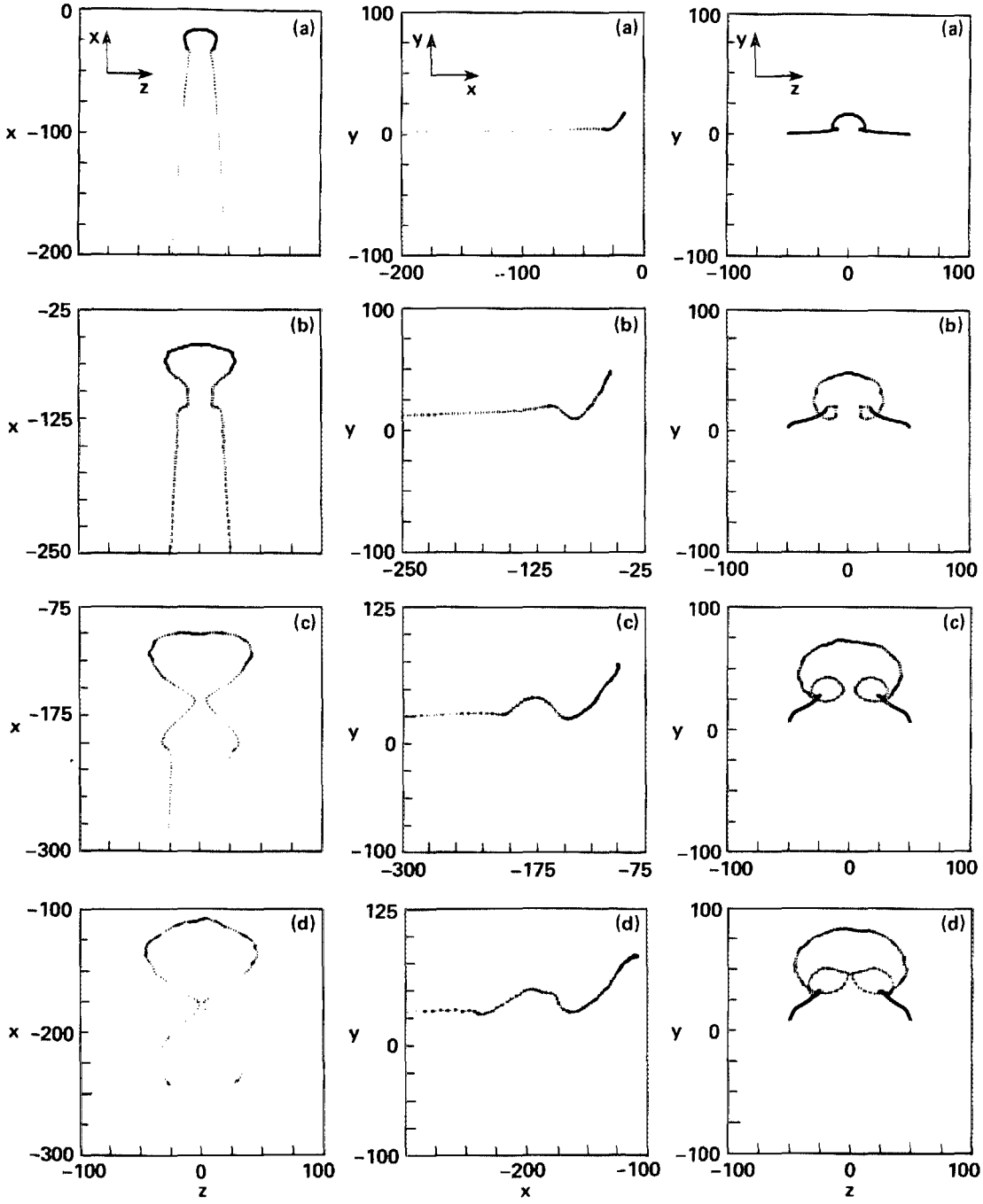

FIG. 3. Evolution of the vortex filament $x = -0.4z^2$, $\sigma = 0.0625$. Plan views are in the left column, the middle column shows the side views, and the end views are shown in the right column: $ta^2\Gamma$ = (a) 1.9×10^3; (b) 1.2×10^4; (c) 2.7×10^4; (d) 3.4×10^4. The symbols indicate the location of the node points.

region progressively evolves into a closed loop resembling a ring vortex.

The calculations are terminated at the nondimensional time $ta^2\Gamma = 6.5\times10^4$, when pinch-off is deemed imminent, and the spatial accuracy of the computations has begun to deteriorate. When the cores of vortices of opposite sign approach each other, viscous diffusion and other fine scale effects become significant. Our inviscid calculations have no provisions for accommodating viscous effects. In the absence of viscous effects and during the final stages of the pinching process, high, localized induced velocities lead to increased vortex stretching and increased local curvature. In fact, numerical studies by Siggia[16] suggest that the final stages of the pinching process at high Reynolds numbers involve intense regions of vortex stretching in which the self-induced motion of opposite-signed vortex filaments generates rapidly increasing filament line lengths, requiring the insertion of a large number of additional computational node points. We see what might be the beginning of such a cascade process in the above Biot–Savart calculations, so that there are strong indications that pinching does occur.

In what follows, we will refer to the time required for the two legs of the filament to most closely approach each other (as allowed by the accuracy of the computations) as the pinching time. Computations with larger core sizes (not shown) could be extended to a point where the two cores actually overlapped without encountering high local curvature in the filament. Note that our estimate of pinch-off time is admittedly crude. Because of numerical errors encountered during the pinching process, this estimate is probably dependent on numerical method and on the number of nodes used. However, in this study we are mainly interested in whether pinching occurs. For further examination of the process itself, more refined techniques, such as that used by Siggia,[16] should be resorted to.

For isolated parabolic filaments, the only nondimensional length scale present is σa. Experiments with different values of σa show that except for a time scale dependence, the pinching process takes place independently of σa and that the nondimensional time for pinch-off depends weakly on σa. Note that the velocity of the filament owing only to *local* induction effects is proportional to $\ln(\rho/\sigma)$. The evolution of the parabolic filament with $a = 0.4$ and $\sigma = 0.0625$ ($\sigma a = 0.025$) is shown in Fig. 3. For this calculation, $N = 321$ node points were used to better resolve the curvature of the filament in the tip region while maintaining the accuracy requirement [Eq. (2b)]. To achieve geometric similarity with the previous case, the range of the variable z was from $z = -50$ to $z = 50$. Once again the filament appears to split into a ring vortex (at $ta^2\Gamma = 3.4\times10^4$). In this calculation, approximately 2.8×10^5 time steps were used. The slight asymmetry developed in the shape of the filament is because of the accumulation of round-off errors. It is interesting that because of the high curvature of the filament near the pinching region, a second ring begins to form just before the section where the first ring is pinched away. The same tendency might have occurred in Fig. 2 if more nodes were used. In the calculations shown in Fig. 2, the ratio of the node spacing and the core radius in the tip region is about 2.5. Thus, strictly one can not use significant-

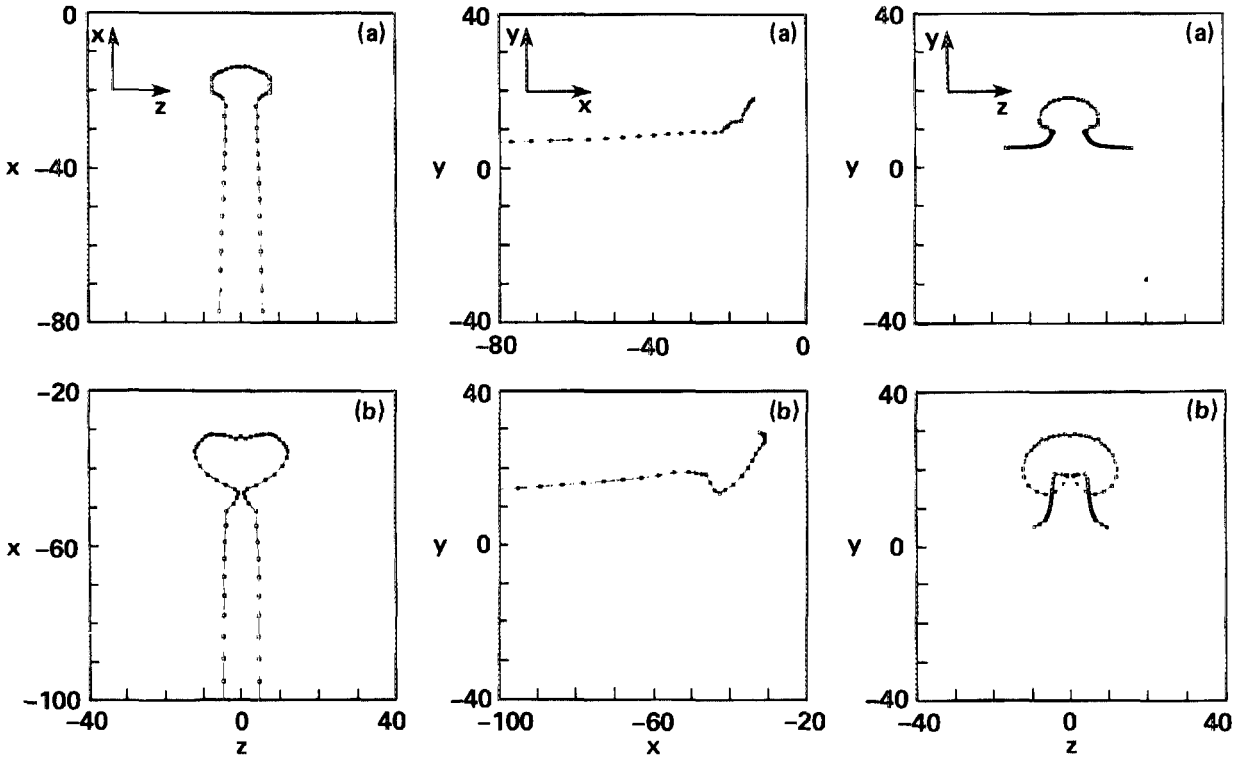

FIG. 4. Evolution of the filament in Fig. 2 initially placed at $y = 5$ and the image vortex placed at $y = -5$: $ta^2\Gamma$ = (a) 7.1×10^3; (b) 2.1×10^4.

ly more node points without violating the accuracy requirement (2b). Despite this, a calculation was carried out with twice as many points ($N = 257$). Once again pinch-off occurred (but at an earlier time) and as in Fig. 3, the early stages of the formation of a second ring were also apparent. All the calculations reported here and others with different parameters (not shown) give the same overall qualitative description of the evolution of the vortex filament. However, because of the inevitable use of *ad hoc* cut-off schemes in the Biot–Savart integral, the quantitative data depends, to some extent, on the spatial computational parameters, i.e., the number of node points and the core diameter.

The above results indicate that the tip region of an isolated parabolic vortex filament resembling a stretched hairpin vortex evolves into a vortex ring.

B. Effect of image vortices

To account for the wall impermeability, an image vortex is introduced into the calculations, which will also introduce another length scale. We will consider the same parabola as that in Fig. 2 ($x = -z^2, \sigma = 0.125$) placed above the wall at $y = 5$. The image vortex is at $y = -5$, and each vortex contains $N = 129$ elements. The evolution of this filament is shown in Fig. 4. The main effect of the impermeable wall or of the image vortex appears to be enhancement of the pinching process. The velocity induced by the image vortex moves the legs of the parabola toward each other. This effect increases as the filament is moved closer to the wall and its image. Note that similar reasonings would indicate that a commonly assumed configuration of the wall layer of turbulent boundary layers consisting of elongated pairs of

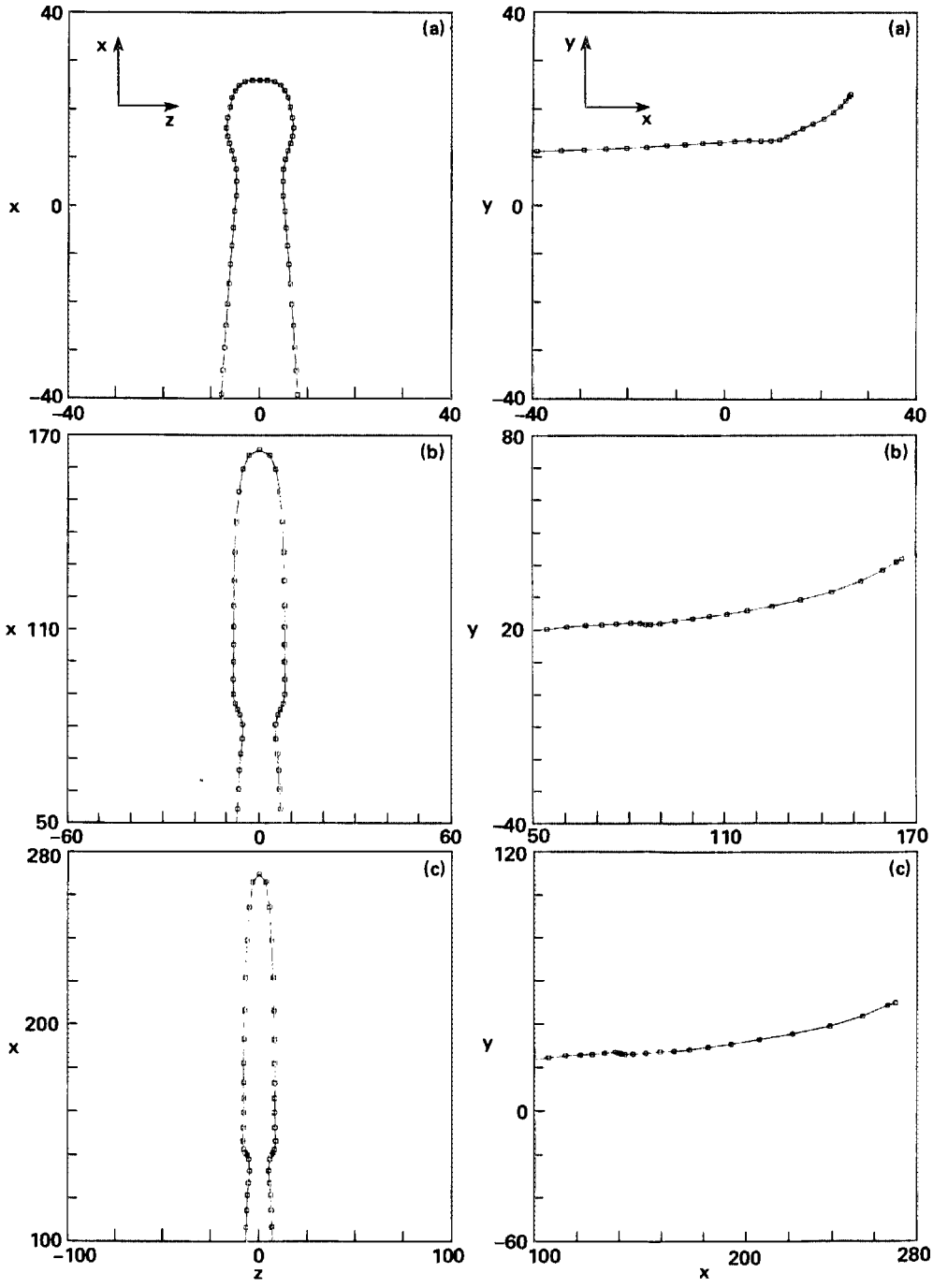

FIG. 5. Evolution of the filament in Fig. 2 in the presence of uniform shear: $ta^2\Gamma =$ (a) 7.1×10^3; (b) 2.1×10^4; (c) 2.8×10^4.

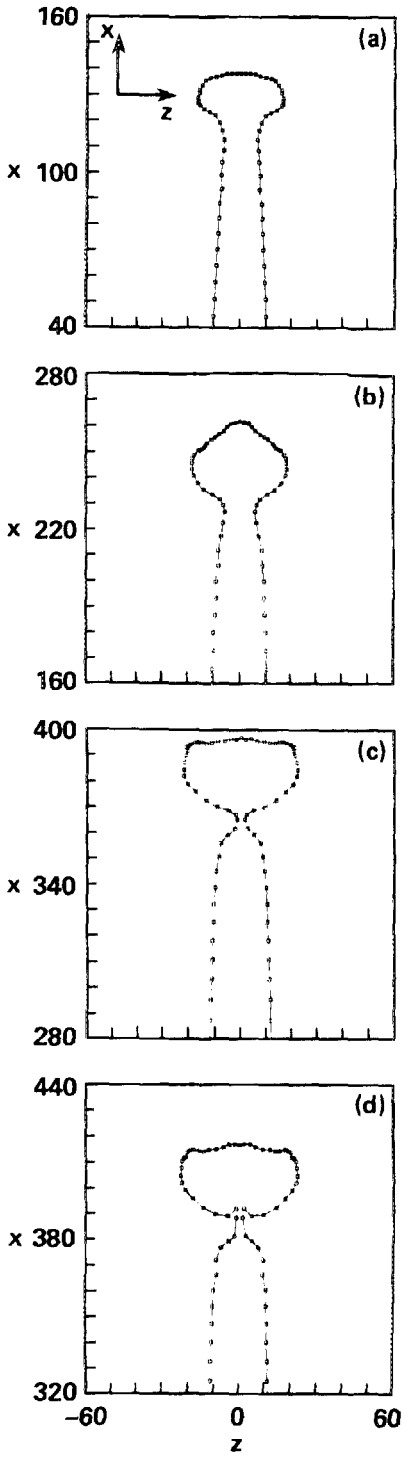

FIG. 6. Evolution of the filament in Fig. 2 in the presence of a boundary-layer-type background shear: $t a^2\Gamma$ = (a) 2.8×10^4; (b) 5.0×10^4; (c) 7.5×10^4; (d) 7.8×10^4.

counter-rotating longitudinal vortices is essentially unstable. That is (depending on whether the flow between the vortices is toward or away from the wall), counter-rotating longitudinal vortices near a wall either merge or move apart.

C. Effect of mean shear

We approximate the effect of mean shear on the vortex filament by adding the mean velocity profile $U(y)$ to the right-hand side of the x component of Eq. (1). As pointed out by Hama[17] and discussed by Aref and Flinchem,[18] this treatment of the background or mean shear is an approximation which neglects the effect of the filament on the background flow. In particular, we neglect the generation of new perturbation vorticity. Aref and Flinchem[18] estimate that the dominant interaction term is the advection of the filament by the background, and the neglected terms are much smaller provided that the diameter of the vortex is negligible compared to the characteristic length scale of the background flow. This condition is valid for the cases considered here. Our estimates using different assumptions are more pessimistic, indicating that the approximation is valid only at early times in the evolution of the vortex. Nevertheless, this approximation is incorporated in calculations reported in the present section.

We shall first consider the case of uniform shear $U(y) = Sy$ (with $S = 0.2$) and the isolated filament ($x = -z^2$, $\sigma = 0.125$). Note that this shear rate is a small fraction of the inverse time scale of the filament's induced motion in the tip region ($\Gamma a^2/S = 150$), and it is significantly smaller than the filament's core vorticity ($\Gamma/(\sigma^2 S) \approx 10^4$).

The results are presented in Fig. 5. When Fig. 5 is compared with Fig. 2, it is clear that the effect of uniform background shear is to inhibit or retard the pinching process. This can be explained by noting that the points with higher y locations on the filament are moved at a faster rate in the x direction than those at lower y values, thus restraining the tip region from taking a circular shape. The effect of stretching by the mean flow is evident; the node points in the tip region are rapidly moved apart.

Next, instead of unform shear, we impose a boundary-layer-type profile,

$$U(y) = c[1 - (0.02y - 1)^6], \quad y < 50,$$
$$U(y) = c, \quad y \geqslant 50,$$

on the filament. With $c = 3.75$, this profile has the same shear rate at $y = 7.5$ (where the filament is placed initially) as in the uniform shear case; but it has smaller shear rates at higher y locations. The evolution of the filament is shown in Fig. 6. The lifted portion of the filament is exposed to lower shear rates, and hence the restraining effect of shear is less pronounced. In agreement with Falco's observations, these results indicate that it is more likely that vortex rings would be detected in the outer region of turbulent boundary layers. It is emphasized that the presence of mean shear is essential for the formation of elongated vortex loops or hairpins with which the calculations were initialized; but the resulting hairpins more readily pinch off into vortex rings in regions with small mean shear.

D. Evolution of a vortex sheet

It is desirable to initialize the computations with a flow structure that occurs often in turbulent boundary layers. In shear flows, the undisturbed mean flow is a continuum of vorticity which is in the form of an infinite sheet of finite thickness. It has been conjectured that a perturbation of this sheet by random velocity fluctuations causes it to roll up into a vortex loop which when stretched appears as a hairpin vortex.[6] The hairpin vortex may then generate a vortex ring

as discussed in the previous sections. The results presented so far were obtained from inviscid Biot–Savart integral calculations that did not acocunt for the effect of viscosity, and for this reason the calculations could not be carried out to the point of actual reconnection. In the Navier–Stokes computations reported in this section the viscous effects are accounted for.

To follow the evolution of an isolated hairpin vortex from its inception, a three-dimensional, time-dependent calculation of the Navier–Stokes equations was carried out. The flow geometry is a channel flow with a constant mean pressure gradient. The Reynolds number based on the centerline mean velocity and channel half-width is about 3500. The initial condition consists of the mean-velocity profile of a fully developed channel flow plus a perturbation in the form of a deformed vortex layer in the lower half of the channel. Using the shear velocity u_τ, obtained from this mean-velocity profile, the wall coordinate of the channel centerline is calculated to be $\delta^+ = \delta u_\tau/\nu = 180$. The computational grid resolutions in the streamwise and spanwise directions are $\Delta x^+ = 18$ and $\Delta z^+ = 6$, respectively. In the normal direction, nonuniform mesh spacing is used which ranges from 0.05 wall units near the wall to 4.4 wall units near the channel centerline.

The vortex lines drawn in the vicinity of the initial perturbation are shown in Fig. (7a). Note that the mean velocity field contains only the spanwise vorticity component, and that departure of the vortex lines from an $(x$-$z)$ plane represents a perturbation. Figures 7(b)–7(d) show the evolution of this perturbed vortex layer. In contrast to the Biot–Savart calculations reported above, vortex lines are traced using the computed velocity field until they intersect the boundaries of the domain or are trapped in a loop.[19] It can be seen that near the vortical structure, vortex lines are stretched and coalesce into vortex tubes, indicating that the initial vortex sheet has rolled up into a hairpin vortex. Figure 7(c) shows that induced motion of the hairpin vortex draws the downstream vortex lines toward itself. Recall that local curvature of the filaments induces velocities in the z direction that produce the characteristic bulged-out, or Ω, shape. When the downstream vortex lines are drawn toward the hairpin vortex, these velocities are enhanced because of the superposition effect, thereby accelerating the pinching process. As shown in Fig. 7(d), these filaments eventually pinch off to form a vortex ring.

The formation of the vortex ring just described is different from the one we discussed in the previous sections: in the previous examples the hairpin vortices themselves deformed into vortex rings, whereas in this example the hairpin vortex creates a vortex ring from the surrounding vortex lines. In both cases, however, the rings are formed because of the induced motion of a curved vortex filament or a hairpin, as discussed in Sec. III A. Examination of the contour plots of the velocity product $(u'v')$ indicates that the vortex ring shown in Fig. 7(d) is associated with high Reynolds shear stress, which is consistent with the measurements of Falco.[10] The point of maximum $(-u'v')$ is located just downstream of the ring.

IV. CONCLUSIONS

We have demonstrated by numerical experiments that a curved filament of concentrated vorticity evolves into a vortex ring as a result of self-induction effects. This result suggests a mechanism for the generation of ring vortices in turbulent shear flows. The ring vortices are more readily

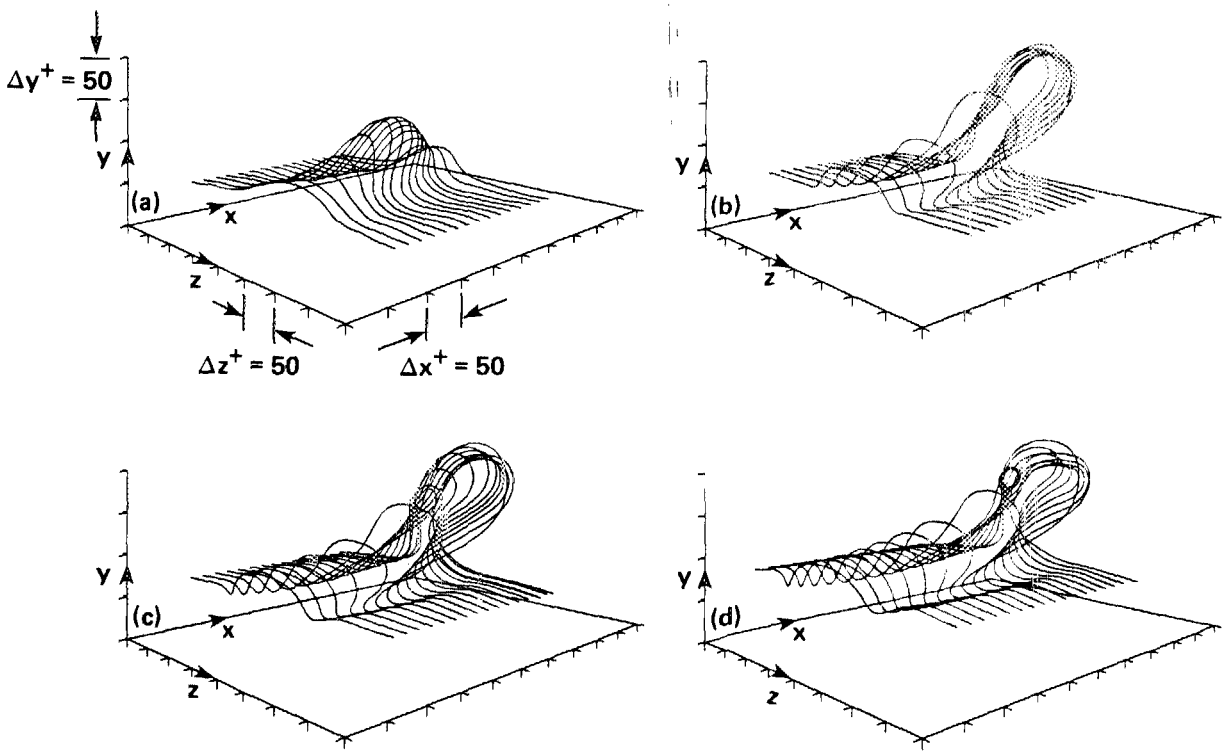

FIG. 7. Evolution of a perturbed vortex layer: tu_τ/δ = (a) 0; (b) 1.2; (c) 1.56; (d) 2.16.

generated in regions with relatively low mean shear. A three-dimensional, unsteady calculation of the Navier–Stokes equations showed that a finite-thickness layer of vorticity, resembling a perturbation to the mean flow in a turbulent boundary layer, rolls up into a hairpin vortex, which in turn produces a vortex ring having high Reynolds shear stress. These results provide a link between Falco's observation of ring vortices in the outer region of turbulent boundary layers and the presence of hairpin vortices reported by others.

The observations of hairpin and ring vortices and the results of the present investigation suggest that in turbulent boundary layers, perturbation of a layer of vorticity leads to its roll-up into filaments of concentrated vorticity. These filaments are then stretched into hairpin vortices. Depending on their lifetimes, the tip region of some of these hairpins may evolve into vortex rings.

ACKNOWLEDGMENTS

We are grateful to Dr. Nagi Mansour and Dr. Robert Rogallo for helpful comments on a draft of this manuscript.

[1]T. Theodorsen, *Proceedings of the 2nd Midwestern Conference on Fluid Mechanics, 17–19 March 1952* (Ohio State University, Columbus, OH, 1952), p. 1.

[2]W. W. Willmarth and B. J. Tu, Phys. Fluids **10**, 134 (1967).

[3]M. R. Head and P. Bandyopadhyay, J. Fluid Mech. **107**, 297 (1981).

[4]J. M. Wallace, in *Developments in Theoretical and Applied Mechanics, XI*, edited by T. J. Chung and G. R. Karr (University of Alabama, Huntsville, AL, 1982), p. 509.

[5]C. R. Smith, in *Proceedings of the Eight Symposium on Turbulence*, edited by G. K. Patterson and J. L. Zakin (University of Missouri, Rolla, 1984), p. 299.

[6]P. Moin and J. Kim, J. Fluid Mech. **155**, 441 (1985).

[7]J. Kim and P. Moin, J. Fluid Mech. **162**, 339 (1986).

[8]P. Moin, M. M. Rogers, and R. D. Moser, in *Proceedings of the Fifth Symposium on Turbulent Shear Flows* (Cornell University, Ithaca, NY, 1985), p. 17.21.

[9]R. E. Falco, AIAA Paper 74–99 (1974).

[10]R. E. Falco, Phys. Fluids **20**, S124 (1977).

[11]F. R. Hama, Phys. Fluids **5**, 1156 (1962).

[12]M. R. Dhanak and B. De Bernardinis, J. Fluid Mech. **109**, 189 (1981).

[13]A. Leonard, J. Comput. Phys. **37**, 289 (1980).

[14]A. Leonard, Ann. Rev. Fluid Mech. **17**, 523 (1985).

[15]P. Moin and J. Kim, J. Comput. Phys. **35**, 381 (1980).

[16]E. D. Siggia, Phys. Fluids **28**, 794 (1985).

[17]F. R. Hama, Phys. Fluids **6**, 526 (1963).

[18]H. Aref and E. P. Flinchem, J. Fluid Mech. **148**, 477 (1984).

[19]In Figs. 7(a) and 7(b) the vortex lines were initiated from different x locations at a fixed y. In addition to these lines, the vortex lines initiated from all the points in the $(x\text{-}y)$ plane bisecting the hairpin-shaped structure were examined. A selection of these lines is shown in Figs. 7(c) and 7(d). In Fig. 7(c) none of these lines formed a loop, whereas in Fig. 7(d) several lines initiated from different grid points formed vortex loops.